Frontiers of Information Technology & Electronic Engineering
www.jzus.zju.edu.cn; engineering.cae.cn; www.springerlink.com
ISSN 2095-9184 (print); ISSN 2095-9230 (online)
E-mail: jzus@zju.edu.cn

Performance analysis on reconfigurable intelligent surface and network-controlled repeater in 3GPP release-18#

Yiwei SUN†1, Boyang DUAN2, Xin SU1, Hanning WANG1, Qi GU1, Jing JIN1, Yifei YUAN†‡1

1Future Research Lab, China Mobile Research Institute, Beijing 100053, China

2School of Information and Communication Engineering, Beijing University of Posts and Telecommunications, Beijing 100876, China

†E-mail: sunyiweiyjy@chinamobile.com; yuanyifei@chinamobile.com

Received May 5, 2023; Revision accepted Aug. 22, 2023; Crosschecked Oct. 30, 2023

Abstract: As a candidate technique to achieve sixth-generation wireless communication (6G), reconfigurable intelligent surface (RIS) has become popular in both academia and industry. For better exploration of the advantages of RIS, we compare the performances of RIS and network-controlled repeater (NCR) in 3GPP release-18. We first theoretically analyze the received signal power and signal-to-noise ratio performances for both RIS and NCR. Then, we simulate the reference signal received power and signal-to-interference-and-noise ratio performances at the system level for both RIS and NCR in the frequency range 1 and frequency range 2 bands. Finally, several insights on engineering applications are given based on the comparison between RIS and NCR.

Key words: Reconfigurable intelligent surface (RIS); Network-controlled repeater (NCR); Standardization; System-level simulation

https://doi.org/10.1631/FITEE.2300321 **CLC number:** TN911

1 Introduction

Opening a new horizon for communications, sixth-generation wireless communication (6G) has promised us various improved performances, including higher data rate and massive connectivity (Gui et al., 2020). To achieve these requirements in 6G, reconfigurable intelligent surface (RIS) is one of the most popular candidates (Basar et al., 2019; Basar, 2020; Tang et al., 2020; RISTA, 2023). However, there are still many lessons to learn from former techniques to find a way to succeed in standardization (Yuan YF et al., 2022). Therefore, a comparison between RIS and network-controlled repeater (NCR) in the most recent 3GPP release-18 (R18) (3GPP, 2022a) is a problem worth researching.

RIS is a cheap, passive artificial structure that can digitally manipulate electromagnetic waves and obtain a preferable electromagnetic propagation environment with limited power consumption (Cui et al., 2014; Hum and Perruisseau-Carrier, 2014). As a promising technique for next-generation communications, RIS has been widely studied by academia (Han et al., 2019; Huang et al., 2019; Wu and Zhang, 2019; Zhang and Zhang, 2020). Han et al. (2019) evaluated the spectral efficiency performance of a RIS-assisted large-scale antenna system by formulating a tight upper bound. To improve energy efficiency, Huang et al. (2019) designed both the transmit power allocation and phase shifts of the RIS subject to individual link budget guarantees for mobile users. In Wu and Zhang (2019), a beamforming scheme for RIS-assisted system was proposed to minimize the total transmit power by jointly optimizing the transmit beamforming by an active

‡ Corresponding author

Electronic supplementary materials: The online version of this article (https://doi.org/10.1631/FITEE.2300321) contains supplementary materials, which are available to authorized users

ORCID: Yiwei SUN, https://orcid.org/0000-0001-8443-6394; Yifei YUAN, https://orcid.org/0000-0002-3474-1865

antenna array and reflect beamforming by passive phase shifters at the RIS. Zhang and Zhang (2020) jointly optimized the RIS reflection coefficients and the multiple-input multiple-output (MIMO) transmit covariance matrix to characterize the fundamental capacity limit of RIS-aided communication systems. Yuan J et al. (2021) and Li et al. (2023a) explored a new modulation scheme in RIS-aided systems. For better improvement in the system performance, vertical Bell Labs layered space-time and Alamouti's schemes have been considered by Khaleel and Basar (2021). Li et al. (2023b) focused on the Internet of Things system. To better analyze the system performance for RIS, channel modeling for RIS-assisted systems is also a hot topic (Basar et al., 2021; Tang et al., 2021; Yildirim et al., 2021). Yildirim et al. (2021) modeled the RIS-assisted system in indoor and outdoor applications and analyzed the rate and bit error ratio performances. To better use the geometry characteristics, Basar et al. (2021) aimed to model a RIS channel model at millimeter-wave frequencies. Moreover, Tang et al. (2021) further modeled the path loss in a RIS-assisted model and verified the model in experimental measurements. Other works (Björnson et al., 2020b; Wu and Zhang, 2020; Pan et al., 2021; Jian et al., 2022) not only summarized the research progress but also pointed out the research direction for RIS in academia. For massive applications in industry, there is still a long way to go for RIS (Liu et al., 2022).

Since RIS often plays the role of relay/repeater in communication systems, the performance comparison between RIS and traditional relays/repeaters naturally draws researchers' attention. Compared with decode-and-forward relay, Björnson et al. (2020a) pointed out that a RIS with a very large array is needed to outperform a decode-and-forward relay in terms of both total transmit power and energy efficiency. Ntontin et al. (2020) compared the RIS with a more general form of relay in terms of rate and energy efficiency; our group has also compared RISs with full/half-duplex relays (Gu et al., 2021). Leone et al. (2022) compared the capacity and reliability of a RIS with those of a smart repeater.

As an evolved repeater, NCR implements a mature technology that has been consolidated over the years (Askar et al., 2021; Qualcomm, 2021). According to previous work (3GPP, 2021), NCR is a single-hop stationary inband radio frequency (RF) repeater used for coverage on the frequency range 1 (FR1) and frequency range 2 (FR2) bands (FR1 and FR2 are the two main frequency ranges for the fifth-generation mobile communication technology (5G); FR1 often refers to sub-6 GHz while FR2 is what we usually call millimeter-wave range). NCR is transparent to user equipments (UEs) and can maintain the gNodeB (gNB)–repeater link and repeater–UE link simultaneously. The technical comparison between RIS and NCR is shown in Table 1. As we can see from Table 1, RIS is different from NCR in terms of both basic and enhanced functions. In terms of basic function, the access link of NCR is not related to the incident beam and is defaulted "OFF" with no influence on the signal, while the backhaul link of NCR can be the same as or different from the control link. In comparison, the access link of RIS is related

Table 1 Technical comparison between RIS and NCR

Function	RIS	NCR
Basic function		
Access link indicator	Relevant to incident beam	Irrelevant to incident beam
Backhaul link indicator	Backhaul link beam probably different from the control link	Backhaul link beam can be the same as or different from the control link
Access link ON/OFF	When OFF, without phase control, mirror reflection	Default "OFF," no influence on the signal
Channel model	Small scale and near field to be researched	Current channel model
Enhanced function		
Energy saving	No amplifiers, strong need	Having amplifiers, no strong need
Channel estimation and feedback	New design under non-transparent channel	No requirement for terminal
Terminal measurement	Introducing terminal measurement, capable of assisting the base station and RIS in joint scheduling	No requirement for terminal

RIS: reconfigurable intelligent surface; NCR: network-controlled repeater

to the incident beam and is defaulted as a mirror reflection, while the backhaul link of RIS probably uses a different beam than the control link. Though NCR implements a mature channel model, the small-scale and near-field channel model still needs further research for RIS. As for the enhanced function, NCR has amplifiers with little need for energy saving and has no special requirements on the terminal for channel estimation, feedback, and terminal measurement. In contrast, RIS has no amplifiers and thus can be greatly energy-saving and may need a new design for channel estimation and feedback under a non-transparent channel. Additionally, RIS introduces terminal measurement, which can assist the base station (BS) and the RIS in joint scheduling. In academia, the comparison between RIS and NCR in various aspects is underway (Ayoubi et al., 2023; Guo et al., 2023). Guo et al. (2023) compared the performances of RIS and NCR at the link level while Ayoubi et al. (2023) focused on coverage in urban scenarios. However, both Ayoubi et al. (2023) and Guo et al. (2023) did not take the geometry of the antenna array into consideration.

In this paper, we compare the performances of RIS and NCR in 3GPP R18. We first model the RIS- and NCR-assisted systems at the signal, array, and channel levels. Then, we theoretically analyze the received signal power and the signal-to-noise ratio (SNR) performances for both RIS and NCR. Moreover, we simulate the reference signal received power (RSRP) and signal-to-interference-and-noise ratio (SINR) performances at the system level for both RIS and NCR in FR1 and FR2 bands. Finally, several insights on engineering applications are given based on the observations of the comparison between RIS and NCR.

The main contributions of this paper are summarized as follows:

1. Geometry of antenna array. Planar array antenna/reflector is widely implemented in engineering practice. To better model the channel in actual scenarios, we consider the geometry of the planar array in the channel model.

2. Different noise characteristics for RIS and NCR. Because of the reflecting ability, RIS does not introduce noise into the system. In contrast, NCR not only introduces but also amplifies the noise. Therefore, we analyze different noise characteristics for RIS and NCR in SNR performance simulation.

3. System-level simulation. In an application scenario, the influence on the whole communication system is the first concern of the engineers. For better guidance in practice, we consider system-level simulation on the system.

The following notations are used throughout this paper: $\boldsymbol{A}$ is a matrix, $\boldsymbol{a}$ is a vector, a is a scalar, and $\mathcal{A}$ is a set. Conjugate transpose and transpose of $\boldsymbol{A}$ are $\boldsymbol{A}^{\mathrm{H}}$ and $\boldsymbol{A}^{\mathrm{T}}$, respectively. $\boldsymbol{I}_N$ denotes an identity matrix with size $N\times N$. $\mathrm{diag}(\boldsymbol{a})$ is a diagonal matrix with every element in vector $\boldsymbol{a}$ as its diagonal elements. Sub-matrix $[\boldsymbol{A}]_{i_1:i_2,j_1:j_2}$ consists of the i_1^{th} to the i_2^{th} rows and the j_1^{th} to the j_2^{th} columns of $\boldsymbol{A}$. Moreover, $\mathrm{mod}(a,2\pi)$ finds the remainder after division for angle a using a modulus of 2π.

2 System models

In this section, we describe the system models for both RIS- and NCR-assisted single-input single-output (SISO) wireless communications.

2.1 Signal model

As shown in Fig. 1a, we consider a RIS-assisted SISO communication system without direct path between the transmitter and the receiver. The RIS is equipped with K_{RIS} ($K_{\mathrm{RIS}}>1$) reflecting elements. The channel between the transmitter and the RIS is denoted as $\boldsymbol{h}_{\mathrm{RIS},1}\in\mathbb{C}^{K_{\mathrm{RIS}}\times 1}$, while the channel between the RIS and the receiver is denoted as $\boldsymbol{h}_{\mathrm{RIS},2}\in\mathbb{C}^{1\times K_{\mathrm{RIS}}}$. Denoting the signal transmitted at the transmitter as s, the received signal at the RIS is

$$\boldsymbol{x}_{\mathrm{RIS}}=\boldsymbol{h}_{\mathrm{RIS},1}s. \tag{1}$$

Considering the reflection coefficients at RIS as $\boldsymbol{\Psi}=[A\exp(\mathrm{j}\psi_1),A\exp(\mathrm{j}\psi_2),\ldots,A\exp(\mathrm{j}\psi_{K_{\mathrm{RIS}}})]^{\mathrm{T}}$, the received signal at the receiver is

$$\begin{aligned} y_{\mathrm{RIS}}=&\boldsymbol{h}_{\mathrm{RIS},2}\mathrm{diag}(\boldsymbol{\Psi})\boldsymbol{x}_{\mathrm{RIS}}+n_{\mathrm{R}}\\ =&\boldsymbol{h}_{\mathrm{RIS},2}\mathrm{diag}(\boldsymbol{\Psi})\boldsymbol{h}_{\mathrm{RIS},1}s+n_{\mathrm{R}}, \end{aligned} \tag{2}$$

where $n_{\mathrm{R}}\in\mathcal{CN}(0,\delta_{\mathrm{R}}^2)$ is the additive white Gaussian noise (AWGN) at the receiver.

In comparison with the RIS-assisted system, we consider an NCR-assisted SISO communication system shown in Fig. 1b. The full duplex relay, NCR, is equipped with K_{NCR} ($K_{\mathrm{NCR}}>1$) antenna elements. Similarly, the channel between the transmitter and the NCR is denoted as $\boldsymbol{h}_{\mathrm{NCR},1}\in\mathbb{C}^{K_{\mathrm{NCR}}\times 1}$, while

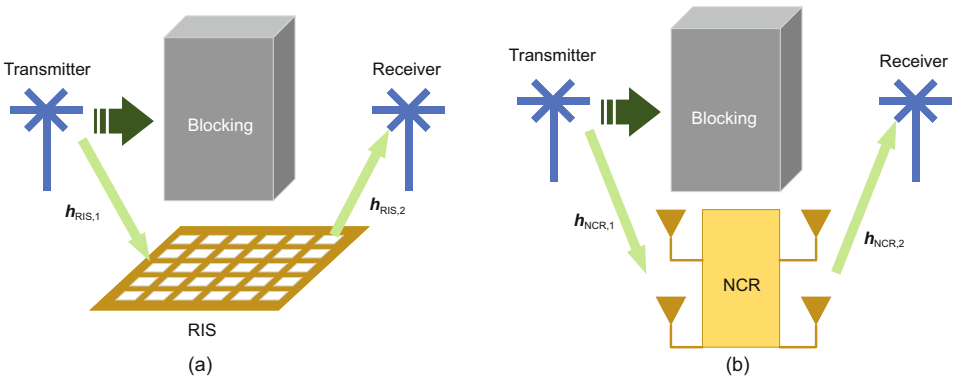

Fig. 1 Illustration of relay-assisted wireless communications without the direct path between the transmitter and the receiver: (a) RIS-assisted; (b) NCR-assisted (RIS: reconfigurable intelligent surface; NCR: network-controlled repeater)

the channel between the NCR and the receiver is denoted as $\boldsymbol{h}_{\mathrm{NCR},2} \in \mathbb{C}^{1\times K_{\mathrm{NCR}}}$. The received signal at the NCR is

$$\boldsymbol{x}_{\mathrm{NCR}} = \boldsymbol{h}_{\mathrm{NCR},1} s + \boldsymbol{n}_{\mathrm{NCR}}, \tag{3}$$

where $\boldsymbol{n}_{\mathrm{NCR}} \in \mathcal{CN}(0, \delta^2 \boldsymbol{I}_{K_{\mathrm{NCR}}})$ is the AWGN at the NCR. Considering the transmission coefficients at the NCR as $\boldsymbol{q} = [q_1 \exp(\mathrm{j}\alpha_1), q_2 \exp(\mathrm{j}\alpha_2), \ldots, q_{K_{\mathrm{NCR}}} \exp(\mathrm{j}\alpha_{K_{\mathrm{NCR}}})]^{\mathrm{T}}$, the received signal at the receiver is

$$\begin{aligned} y_{\mathrm{NCR}} =& \boldsymbol{h}_{\mathrm{NCR},2} \mathrm{diag}(\boldsymbol{q}) \boldsymbol{x}_{\mathrm{NCR}} + n_{\mathrm{R}} \\ =& \boldsymbol{h}_{\mathrm{RIS},2} \mathrm{diag}(\boldsymbol{q})(\boldsymbol{h}_{\mathrm{NCR},1} s + \boldsymbol{n}_{\mathrm{NCR}}) + n_{\mathrm{R}}. \end{aligned} \tag{4}$$

Notice that the NCR is with AWGN and is able to magnify the received signal at the NCR. How these two biggest differences in comparison to the RIS influence the performance of NCR is to be researched in the remainder of the paper.

2.2 Antenna model

We consider that the relay is equipped with a planar array reflector/antenna shown in Fig. 2. Ignoring the direct link between the transmitter and the receiver, we focus on the free-space path loss modeling. Consider a Cartesian coordinate system with the origin at the center of the planar array and the x-y plane on the planar array. The coordinates of the transmitter and the receiver are $(x_{\mathrm{T}}, y_{\mathrm{T}}, z_{\mathrm{T}})$ and $(x_{\mathrm{R}}, y_{\mathrm{R}}, z_{\mathrm{R}})$, respectively. We assume that the positions of the transmitter and the receiver are the same for both RIS and NCR. For the RIS relay, we denote the numbers of rows and columns of regularly arranged unit cells as N_{RIS} and M_{RIS} respectively,

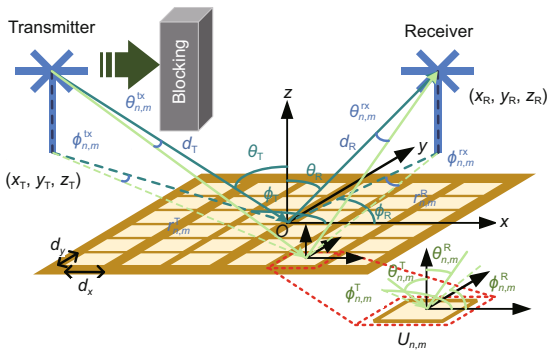

Fig. 2 Illustration of relay-assisted wireless communications with a planar array

where $N_{\mathrm{RIS}} M_{\mathrm{RIS}} = K_{\mathrm{RIS}}$. In comparison, we denote the numbers of rows and columns of regularly arranged unit cells for the NCR relay as N_{NCR} and M_{NCR} respectively, where $N_{\mathrm{NCR}} M_{\mathrm{NCR}} = K_{\mathrm{NCR}}$. To simplify, the numbers of rows and columns for the planar array are denoted as N and M, respectively. Without losing generality, we assume that both N and M are even numbers. For each unit $U_{n,m}$ on the n^{th} row and the m^{th} column, the sizes along the x axis and the y axis are $d_x \in [\frac{\lambda}{10}, \frac{\lambda}{2}]$ and $d_y \in [\frac{\lambda}{10}, \frac{\lambda}{2}]$ respectively, where λ is the wavelength. We assume that the sizes of each unit $U_{n,m}$ are the same for both RIS and NCR. The center position of the unit $U_{n,m}$ is $((m-\frac{1}{2})d_x, (n-\frac{1}{2})d_y, 0)$, where $m \in [1-\frac{M}{2}, \frac{M}{2}]$ and $n \in [1-\frac{N}{2}, \frac{N}{2}]$. We denote the distance between the transmitter and the center of the planar array, the distance between the receiver and the center of the planar array, the elevation angle and the azimuth angle to the transmitter, and the elevation angle and the azimuth angle to the receiver as d_{T}, d_{R}, θ_{T}, ϕ_{T}, θ_{R}, ϕ_{R}, respectively. For each unit $U_{n,m}$ on the n^{th}

row and the m^{th} column, the distance between the transmitter and $U_{n,m}$, the distance between the receiver and $U_{n,m}$, the elevation angle and the azimuth angle from $U_{n,m}$ to the transmitter, and the elevation angle and the azimuth angle from $U_{n,m}$ to the receiver are denoted as $r^{\mathrm{T}}_{n,m}$, $r^{\mathrm{R}}_{n,m}$, $\theta^{\mathrm{T}}_{n,m}$, $\phi^{\mathrm{T}}_{n,m}$, $\theta^{\mathrm{R}}_{n,m}$, $\phi^{\mathrm{R}}_{n,m}$, respectively.

For RIS, the power radiation pattern of each unit cell is denoted as $F_{\mathrm{RIS}}(\theta,\phi)$, which reveals the dependence of the power density of the unit cell on the angle of departure/arrival. Assuming 100% antenna efficiency, the gain of the unit cell is defined as

$$G_{\mathrm{RIS}}=\frac{4\pi}{\int_{\phi=0}^{2\pi}\int_{\theta=0}^{\pi}F_{\mathrm{RIS}}(\theta,\phi)\sin\theta\mathrm{d}\theta\mathrm{d}\phi}, \tag{5}$$

which is related only to the normalized power radiation pattern $F_{\mathrm{RIS}}(\theta,\phi)$. Similarly for NCR, we define the power radiation pattern and the gain for the unit cell as $F_{\mathrm{NCR}}(\theta,\phi)$ and G_{NCR}, respectively. Again, under the assumption of 100% antenna efficiency, the relationship between $F_{\mathrm{NCR}}(\theta,\phi)$ and G_{NCR} is

$$G_{\mathrm{NCR}}=\frac{4\pi}{\int_{\phi=0}^{2\pi}\int_{\theta=0}^{\pi}F_{\mathrm{NCR}}(\theta,\phi)\sin\theta\mathrm{d}\theta\mathrm{d}\phi}. \tag{6}$$

We consider that the transmitter emits the signal to the relay with power P_{T} through the antenna with normalized power radiation pattern $F_{\mathrm{T}}(\theta,\phi)$ and antenna gain G_{T}. As for the receiver, the normalized power radiation pattern and antenna gain are $F_{\mathrm{R}}(\theta,\phi)$ and G_{R}, respectively. The elevation and azimuth angles from the transmitting antenna to the unit $U_{n,m}$ and the elevation and azimuth angles from the receiving antenna to the unit $U_{n,m}$ are $\theta^{\mathrm{tx}}_{n,m}$, $\phi^{\mathrm{tx}}_{n,m}$, $\theta^{\mathrm{rx}}_{n,m}$, and $\phi^{\mathrm{rx}}_{n,m}$, respectively. In this study, perfect match is assumed in polarization for both the transmitter and the receiver after relay.

Additionally, the reflection/transmission coefficient vector can be expressed in the matrix form because of the application of planar array. For RIS, the reflection coefficients can be expressed as $\boldsymbol{\Gamma}$, where $\mathrm{vec}(\boldsymbol{\Gamma})=\boldsymbol{\Psi}$. Denoting $\boldsymbol{\Gamma}=[A\exp(\mathrm{j}\psi_{n,m})]_{n=1:N_{\mathrm{RIS}}}^{m=1:M_{\mathrm{RIS}}}$, the relation between the elements in $\boldsymbol{\Gamma}$ and $\boldsymbol{\Psi}$ is $\psi_{n,m}=\psi_{(n-1)M_{\mathrm{RIS}}+m}$. For NCR, the transmission coefficients can be expressed as $\boldsymbol{Q}$, where $\mathrm{vec}(\boldsymbol{Q})=\boldsymbol{q}$. Denoting $\boldsymbol{Q}=[q_{n,m}\exp(\mathrm{j}\alpha_{n,m})]_{n=1:N_{\mathrm{NCR}}}^{m=1:M_{\mathrm{NCR}}}$, the relations between the elements in $\boldsymbol{Q}$ and $\boldsymbol{q}$ are $q_{n,m}=q_{(n-1)M_{\mathrm{NCR}}+m}$ and $\alpha_{n,m}=\alpha_{(n-1)M_{\mathrm{NCR}}+m}$.

2.3 Channel model

We consider the most widely used model defined in 3GPP TR 38.901 (3GPP, 2022b) for channel modeling in the system-level simulation. In a practical outdoor scenario, the relay is often deployed higher than users and can be regarded as a node in far-field assumption. Therefore, many aspects, such as path loss, antenna polarization, and the phase difference at different positions of a continuous surface, are similar to those for the channel model in 3GPP TR 38.901. For simplicity, both transmitter–relay and relay–receiver links consider a line-of-sight path according to the system model.

3 Theoretical performance analysis

In this section, we compare the performances in received signal power and SNR for both RIS and NCR in the far-field case.

3.1 RIS: received power and SNR

Consider the case in which both the transmitter and the receiver are in the far field of the RIS. Both the incident beams at the relay and the receiver can be seen as plane waves; thus, the phase on each unit cell is unified. Assume that the directions of peak radiation of both the transmitting and the receiving antennas point to the center of the RIS. Considering perfect beamforming, the received signal power at the receiver through the RIS can be written as Eq. (7) (on top of the next page, wherein $\epsilon_1^{\mathrm{RIS}}(m-1/2)\,d_x+\epsilon_2^{\mathrm{RIS}}(n-1/2)\,d_y=\lambda\psi_{n,m}/(2\pi)$) according to Proposition 2 in Tang et al. (2021). We can achieve maximizing Eq. (7) as Eq. (8) (on top of the next page) when $\epsilon_1^{\mathrm{RIS}}=-\sin\theta_{\mathrm{T}}\cos\phi_{\mathrm{T}}-\sin\theta_{\mathrm{R}}\cos\phi_{\mathrm{R}}$ and $\epsilon_2^{\mathrm{RIS}}=-\sin\theta_{\mathrm{T}}\sin\phi_{\mathrm{T}}-\sin\theta_{\mathrm{R}}\sin\phi_{\mathrm{R}}$. Correspondingly, the optimal RIS reflected phase coefficient design is

$$\begin{aligned}\psi_{n,m}=&\mathrm{mod}\left(\frac{2\pi}{\lambda}\left(\epsilon_1^{\mathrm{RIS}}\left(m-\frac{1}{2}\right)d_x\right.\right.\\&\left.\left.+\epsilon_2^{\mathrm{RIS}}\left(n-\frac{1}{2}\right)d_y\right),2\pi\right).\end{aligned} \tag{9}$$

According to Eq. (8), the gain by RIS is

$$G_{\mathrm{RIS}}A^2F_{\mathrm{RIS}}(\theta_{\mathrm{T}},\phi_{\mathrm{T}})F_{\mathrm{RIS}}(\theta_{\mathrm{R}},\phi_{\mathrm{R}})M_{\mathrm{RIS}}^2N_{\mathrm{RIS}}^2d_xd_y. \tag{10}$$

We can see that the gain by RIS comes from four main aspects: (1) the transmitting power of RIS;

$$P_{\mathrm{RIS}}=P_{\mathrm{T}}\frac{G_{\mathrm{T}}G_{\mathrm{R}}G_{\mathrm{RIS}}M_{\mathrm{RIS}}^2N_{\mathrm{RIS}}^2d_xd_y\lambda^2F_{\mathrm{RIS}}(\theta_{\mathrm{T}},\phi_{\mathrm{T}})F_{\mathrm{RIS}}(\theta_{\mathrm{R}},\phi_{\mathrm{R}})A^2}{64\pi^3d_{\mathrm{T}}^2d_{\mathrm{R}}^2}\left|\frac{\mathrm{sinc}\left(\frac{M_{\mathrm{RIS}}\pi}{\lambda}(\sin\theta_{\mathrm{T}}\cos\phi_{\mathrm{T}}+\sin\theta_{\mathrm{R}}\cos\phi_{\mathrm{R}}+\epsilon_1^{\mathrm{RIS}})d_x\right)}{\mathrm{sinc}\left(\frac{\pi}{\lambda}(\sin\theta_{\mathrm{T}}\cos\phi_{\mathrm{T}}+\sin\theta_{\mathrm{R}}\cos\phi_{\mathrm{R}}+\epsilon_1^{\mathrm{RIS}})d_x\right)}\right.$$
$$\left.\cdot\frac{\mathrm{sinc}\left(\frac{N_{\mathrm{RIS}}\pi}{\lambda}(\sin\theta_{\mathrm{T}}\sin\phi_{\mathrm{T}}+\sin\theta_{\mathrm{R}}\sin\phi_{\mathrm{R}}+\epsilon_2^{\mathrm{RIS}})d_y\right)}{\mathrm{sinc}\left(\frac{\pi}{\lambda}(\sin\theta_{\mathrm{T}}\sin\phi_{\mathrm{T}}+\sin\theta_{\mathrm{R}}\sin\phi_{\mathrm{R}}+\epsilon_2^{\mathrm{RIS}})d_y\right)}\right|^2. \tag{7}$$

$$P_{\mathrm{RIS}}^{\max}=P_{\mathrm{T}}\frac{G_{\mathrm{T}}G_{\mathrm{R}}G_{\mathrm{RIS}}M_{\mathrm{RIS}}^2N_{\mathrm{RIS}}^2d_xd_y\lambda^2F_{\mathrm{RIS}}(\theta_{\mathrm{T}},\phi_{\mathrm{T}})F_{\mathrm{RIS}}(\theta_{\mathrm{R}},\phi_{\mathrm{R}})A^2}{64\pi^3d_{\mathrm{T}}^2d_{\mathrm{R}}^2}. \tag{8}$$

(2) antenna gain of a single-array element; (3) directional diagram of a single-array element; (4) beamforming.

Given the RIS-based relay system model in Eq. (2), the received noise power for RIS is $P_{\mathrm{RIS}}^{\mathrm{N}}=\delta_{\mathrm{R}}^2$. The maximum SNR for RIS can be expressed as Eq. (11) (on top of the next page).

The received power and SNR are two important performance metrics for the system. Therefore, we derive the received power and SNR for NCR compared to RIS in the following context.

3.2 NCR: received power deduction

We first derive the received power at NCR from the transmitter.

Proposition 1 Assume that the direction of peak radiation of the transmitting antenna points to the center of the NCR, and that the receiving beamforming coefficient vector for the NCR is $\boldsymbol{u}=\mathrm{vec}([\exp(\mathrm{j}\beta_{n,m})]_{n=1:N_{\mathrm{NCR}}}^{m=1:M_{\mathrm{NCR}}})$. The received power at the NCR is

$$P^{(1)}=P_{\mathrm{T}}\frac{G_{\mathrm{T}}M_{\mathrm{NCR}}^2N_{\mathrm{NCR}}^2F_{\mathrm{NCR}}(\theta_{\mathrm{T}},\phi_{\mathrm{T}})d_xd_y}{4\pi d_{\mathrm{T}}^2}\cdot\left|\frac{\mathrm{sinc}\left(\frac{M_{\mathrm{NCR}}\pi}{\lambda}(\sin\theta_{\mathrm{T}}\cos\phi_{\mathrm{T}}+\epsilon_1^{\mathrm{NCR}})d_x\right)}{\mathrm{sinc}\left(\frac{\pi}{\lambda}(\sin\theta_{\mathrm{T}}\cos\phi_{\mathrm{T}}+\epsilon_1^{\mathrm{NCR}})d_x\right)}\right.$$
$$\left.\cdot\frac{\mathrm{sinc}\left(\frac{N_{\mathrm{NCR}}\pi}{\lambda}(\sin\theta_{\mathrm{T}}\sin\phi_{\mathrm{T}}+\epsilon_2^{\mathrm{NCR}})d_y\right)}{\mathrm{sinc}\left(\frac{\pi}{\lambda}(\sin\theta_{\mathrm{T}}\sin\phi_{\mathrm{T}}+\epsilon_2^{\mathrm{NCR}})d_y\right)}\right|^2, \tag{12}$$

where $\lambda\beta_{n,m}/(2\pi)=\epsilon_1^{\mathrm{NCR}}(m-1/2)d_x+\epsilon_2^{\mathrm{NCR}}(n-1/2)d_y$. When $\epsilon_1^{\mathrm{NCR}}=-\sin\theta_{\mathrm{T}}\cos\phi_{\mathrm{T}}$ and $\epsilon_2^{\mathrm{NCR}}=-\sin\theta_{\mathrm{T}}\sin\phi_{\mathrm{T}}$, the maximum received power at the NCR can be achieved as

$$P_{\max}^{(1)}=P_{\mathrm{T}}\frac{G_{\mathrm{T}}M_{\mathrm{NCR}}^2N_{\mathrm{NCR}}^2d_xd_yF_{\mathrm{NCR}}(\theta_{\mathrm{T}},\phi_{\mathrm{T}})}{4\pi d_{\mathrm{T}}^2}. \tag{13}$$

Correspondingly, the beamforming coefficient at unit $U_{n,m}$ is

$$\begin{aligned}\beta_{n,m}=&\frac{2\pi}{\lambda}\left(\epsilon_1^{\mathrm{NCR}}\left(m-\frac{1}{2}\right)d_x+\epsilon_2^{\mathrm{NCR}}\left(n-\frac{1}{2}\right)d_y\right)\\=&-\frac{2\pi}{\lambda}\left(\left(m-\frac{1}{2}\right)d_x\sin\theta_{\mathrm{T}}\cos\phi_{\mathrm{T}}\right.\\&\left.+\left(n-\frac{1}{2}\right)d_y\sin\theta_{\mathrm{T}}\sin\phi_{\mathrm{T}}\right).\end{aligned} \tag{14}$$

The proof of Proposition 1 is provided in the supplementary materials.

As we can see from the proof of Proposition 1, the gain of NCR comes from three main aspects: (1) aperture size of the NCR; (2) directional diagram of a single-array element; (3) beamforming.

For the NCR–receiver link, we have the following proposition:

Proposition 2 Assume that the maximum received power at the NCR in Proposition 1 can be achieved, that the direction of peak radiation of the receiving antenna points to the center of the NCR, and that the received power at the NCR is uniformly distributed to every array element when transmitting to the receiver. Without loss of generality, the transmission coefficients of all unit cells at the NCR have unified amplitude B and different phase shifts $\alpha_{n,m}$. The received power at the receiver is shown in Eq. (15) (on top of the next page), where $\epsilon_3^{\mathrm{NCR}}(m-1/2)d_x+\epsilon_4^{\mathrm{NCR}}(n-1/2)d_y=\lambda\alpha_{n,m}/(2\pi)$. When $\epsilon_3^{\mathrm{NCR}}=-\sin\theta_{\mathrm{R}}\cos\phi_{\mathrm{R}}$ and $\epsilon_4^{\mathrm{NCR}}=-\sin\theta_{\mathrm{R}}\sin\phi_{\mathrm{R}}$, the maximum received power at the NCR can be achieved as Eq. (16) (on top of the next page). Correspondingly, the transmission coefficient at unit $U_{n,m}$ is

$$\alpha_{n,m}=\frac{2\pi}{\lambda}\left(\epsilon_3^{\mathrm{NCR}}\left(m-\frac{1}{2}\right)d_x+\epsilon_4^{\mathrm{NCR}}\left(n-\frac{1}{2}\right)d_y\right)$$

$$\gamma_{\mathrm{RIS}}=\frac{P_{\mathrm{RIS}}^{\max}}{P_{\mathrm{RIS}}^{\mathrm{N}}}=P_{\mathrm{T}}\frac{G_{\mathrm{T}}G_{\mathrm{R}}G_{\mathrm{RIS}}M_{\mathrm{RIS}}^{2}N_{\mathrm{RIS}}^{2}d_x d_y\lambda^{2}F_{\mathrm{RIS}}(\theta_{\mathrm{T}},\phi_{\mathrm{T}})F_{\mathrm{RIS}}(\theta_{\mathrm{R}},\phi_{\mathrm{R}})A^{2}}{64\pi^{3}\delta_{\mathrm{R}}^{2}d_{\mathrm{T}}^{2}d_{\mathrm{R}}^{2}}. \tag{11}$$

$$P_{\mathrm{NCR}}=P_{\mathrm{T}}\frac{G_{\mathrm{T}}G_{\mathrm{R}}G_{\mathrm{NCR}}M_{\mathrm{NCR}}^{3}N_{\mathrm{NCR}}^{3}d_x d_y\lambda^{2}F_{\mathrm{NCR}}(\theta_{\mathrm{T}},\phi_{\mathrm{T}})F_{\mathrm{NCR}}(\theta_{\mathrm{R}},\phi_{\mathrm{R}})B}{64\pi^{3}d_{\mathrm{T}}^{2}d_{\mathrm{R}}^{2}}\left|\frac{\mathrm{sinc}\left(\frac{M_{\mathrm{NCR}}\pi}{\lambda}(\sin\theta_{\mathrm{R}}\cos\phi_{\mathrm{R}}+\epsilon_{3}^{\mathrm{NCR}})d_x\right)}{\mathrm{sinc}\left(\frac{\pi}{\lambda}(\sin\theta_{\mathrm{R}}\cos\phi_{\mathrm{R}}+\epsilon_{3}^{\mathrm{NCR}})d_x\right)}\right.$$
$$\left.\cdot\frac{\mathrm{sinc}\left(\frac{N_{\mathrm{NCR}}\pi}{\lambda}(\sin\theta_{\mathrm{R}}\sin\phi_{\mathrm{R}}+\epsilon_{4}^{\mathrm{NCR}})d_y\right)}{\mathrm{sinc}\left(\frac{\pi}{\lambda}(\sin\theta_{\mathrm{R}}\sin\phi_{\mathrm{R}}+\epsilon_{4}^{\mathrm{NCR}})d_y\right)}\right|^{2}. \tag{15}$$

$$P_{\mathrm{NCR}}^{\max}=P_{\mathrm{T}}\frac{G_{\mathrm{T}}G_{\mathrm{R}}G_{\mathrm{NCR}}M_{\mathrm{NCR}}^{3}N_{\mathrm{NCR}}^{3}d_x d_y\lambda^{2}F_{\mathrm{NCR}}(\theta_{\mathrm{T}},\phi_{\mathrm{T}})F_{\mathrm{NCR}}(\theta_{\mathrm{R}},\phi_{\mathrm{R}})B}{64\pi^{3}d_{\mathrm{T}}^{2}d_{\mathrm{R}}^{2}}. \tag{16}$$

$$\begin{aligned}=&-\frac{2\pi}{\lambda}\left(\left(m-\frac{1}{2}\right)d_x\sin\theta_{\mathrm{R}}\cos\phi_{\mathrm{R}}\right.\\&\left.+\left(n-\frac{1}{2}\right)d_y\sin\theta_{\mathrm{R}}\sin\phi_{\mathrm{R}}\right).\end{aligned} \tag{17}$$

The proof of Proposition 2 is provided in the supplementary materials.

As we can see from the proof of Proposition 2, the gain of NCR can be written as

$$G_{\mathrm{NCR}}BF_{\mathrm{NCR}}(\theta_{\mathrm{T}},\phi_{\mathrm{T}})F_{\mathrm{NCR}}(\theta_{\mathrm{R}},\phi_{\mathrm{R}})M_{\mathrm{NCR}}^{3}N_{\mathrm{NCR}}^{3}d_x dy, \tag{18}$$

which comes from four main aspects: (1) the transmitting power of NCR; (2) antenna gain of a single-array element; (3) directional diagram of a single-array element; (4) beamforming.

3.3 NCR: SNR with magnified AWGN

Comparing the NCR system model in Eq. (4) with the RIS model in Eq. (2), NCR introduces extra noise and magnifies the extra noise brought in by itself. After power allocation and transmitting beamforming, the noise of NCR is no longer AWGN but color noise. Therefore, we theoretically analyze the influence by the NCR in the following context:

Assuming that all the array units contribute to the AWGN of NCR uniformly, the transmission noise power of NCR is

$$P_{n,m}^{\mathrm{N,tx}}=B|\exp(\mathrm{j}\alpha_{n,m})|^{2}\frac{\delta^{2}}{N_{\mathrm{NCR}}M_{\mathrm{NCR}}}. \tag{19}$$

The corresponding electric field is

$$E_{n,m}^{\mathrm{N}}=\sqrt{\frac{8\pi Z_0 P_{n,m}^{\mathrm{N,tx}}}{G_{\mathrm{R}}\lambda^{2}}}\exp\left(\frac{-\mathrm{j}2\pi}{\lambda}r_{n,m}^{\mathrm{R}}\right)$$
$$=\sqrt{\frac{8\pi Z_0 B\delta^{2}}{G_{\mathrm{R}}\lambda^{2}N_{\mathrm{NCR}}M_{\mathrm{NCR}}}}\exp\left(\mathrm{j}\alpha_{n,m}-\frac{\mathrm{j}2\pi}{\lambda}r_{n,m}^{\mathrm{R}}\right), \tag{20}$$

where Z_0 is the characteristic impedance of the air. Then, the received noise power generated by the NCR is

$$P_{\mathrm{NCR}}^{\mathrm{N,rx}}=\delta^{2}\frac{G_{\mathrm{R}}G_{\mathrm{NCR}}\lambda^{2}F_{\mathrm{NCR}}(\theta_{\mathrm{R}},\phi_{\mathrm{R}})B}{16\pi^{2}d_{\mathrm{R}}^{2}N_{\mathrm{NCR}}M_{\mathrm{NCR}}}$$
$$\cdot\left|\sum_{m=1-\frac{M_{\mathrm{NCR}}}{2}}^{\frac{M_{\mathrm{NCR}}}{2}}\sum_{n=1-\frac{N_{\mathrm{NCR}}}{2}}^{\frac{N_{\mathrm{NCR}}}{2}}\exp\left(\mathrm{j}\left(\alpha_{n,m}-\frac{2\pi}{\lambda}r_{n,m}^{\mathrm{R}}\right)\right)\right|^{2}. \tag{21}$$

Similar to the proofs of Propositions 1 and 2, the maximum received noise power generated by the NCR is

$$\max(P_{\mathrm{NCR}}^{\mathrm{N,rx}})=\delta^{2}\frac{G_{\mathrm{R}}G_{\mathrm{NCR}}N_{\mathrm{NCR}}M_{\mathrm{NCR}}\lambda^{2}F_{\mathrm{NCR}}(\theta_{\mathrm{R}},\phi_{\mathrm{R}})B}{16\pi^{2}d_{\mathrm{R}}^{2}}. \tag{22}$$

As we can see in Eq. (22), NCR can magnify its own noise by

$$\frac{\max(P_{\mathrm{NCR}}^{\mathrm{N,rx}})}{\delta^{2}}=\frac{G_{\mathrm{R}}G_{\mathrm{NCR}}N_{\mathrm{NCR}}M_{\mathrm{NCR}}\lambda^{2}F_{\mathrm{NCR}}(\theta_{\mathrm{R}},\phi_{\mathrm{R}})B}{16\pi^{2}d_{\mathrm{R}}^{2}}. \tag{23}$$

Thus, the total received noise power is

$$P_{\mathrm{NCR}}^{\mathrm{N}}=\delta_{\mathrm{R}}^{2}+\delta^{2}\frac{G_{\mathrm{R}}G_{\mathrm{NCR}}N_{\mathrm{NCR}}M_{\mathrm{NCR}}\lambda^{2}F_{\mathrm{NCR}}(\theta_{\mathrm{R}},\phi_{\mathrm{R}})B}{16\pi^{2}d_{\mathrm{R}}^{2}}. \tag{24}$$

Then, the SNR for NCR is shown in Eq. (25) (on top of the next page).

3.4 Comparison of RIS and NCR

According to the above deduction, we analyze the differences between RIS- and NCR-based relay systems in terms of both received power and SNR.

$$\gamma_{\mathrm{NCR}}=\frac{P_{\mathrm{NCR}}^{\max}}{P_{\mathrm{NCR}}^{\mathrm{N}}}=P_{\mathrm{T}}\frac{G_{\mathrm{T}}G_{\mathrm{R}}G_{\mathrm{NCR}}M_{\mathrm{NCR}}^{3}N_{\mathrm{NCR}}^{3}d_x d_y\lambda^2F_{\mathrm{NCR}}(\theta_{\mathrm{T}},\phi_{\mathrm{T}})F_{\mathrm{NCR}}(\theta_{\mathrm{R}},\phi_{\mathrm{R}})B}{64\pi^3\delta_{\mathrm{R}}^2d_{\mathrm{T}}^2d_{\mathrm{R}}^2+4\pi\delta^2d_{\mathrm{T}}^2G_{\mathrm{R}}G_{\mathrm{NCR}}M_{\mathrm{NCR}}N_{\mathrm{NCR}}\lambda^2F_{\mathrm{NCR}}(\theta_{\mathrm{R}},\phi_{\mathrm{R}})B}. \tag{25}$$

$$\frac{P_{\mathrm{RIS}}^{\max}}{P_{\mathrm{NCR}}^{\max}}=\frac{G_{\mathrm{RIS}}M_{\mathrm{RIS}}^{2}N_{\mathrm{RIS}}^{2}F_{\mathrm{RIS}}(\theta_{\mathrm{T}},\phi_{\mathrm{T}})F_{\mathrm{RIS}}(\theta_{\mathrm{R}},\phi_{\mathrm{R}})A^2}{G_{\mathrm{NCR}}M_{\mathrm{NCR}}^{3}N_{\mathrm{NCR}}^{3}F_{\mathrm{NCR}}(\theta_{\mathrm{T}},\phi_{\mathrm{T}})F_{\mathrm{NCR}}(\theta_{\mathrm{R}},\phi_{\mathrm{R}})B}. \tag{26}$$

$$\frac{\gamma_{\mathrm{RIS}}}{\gamma_{\mathrm{NCR}}}=\frac{(16\pi^2\delta_{\mathrm{R}}^2d_{\mathrm{R}}^2+\delta^2G_{\mathrm{R}}G_{\mathrm{NCR}}M_{\mathrm{NCR}}N_{\mathrm{NCR}}\lambda^2F_{\mathrm{NCR}}(\theta_{\mathrm{R}},\phi_{\mathrm{R}})B)G_{\mathrm{RIS}}M_{\mathrm{RIS}}^{2}N_{\mathrm{RIS}}^{2}F_{\mathrm{RIS}}(\theta_{\mathrm{T}},\phi_{\mathrm{T}})F_{\mathrm{RIS}}(\theta_{\mathrm{R}},\phi_{\mathrm{R}})A^2}{16\pi^2d_{\mathrm{R}}^2G_{\mathrm{NCR}}M_{\mathrm{NCR}}^{3}N_{\mathrm{NCR}}^{3}F_{\mathrm{NCR}}(\theta_{\mathrm{T}},\phi_{\mathrm{T}})F_{\mathrm{NCR}}(\theta_{\mathrm{R}},\phi_{\mathrm{R}})B}. \tag{27}$$

For received power, the ratio of RIS to NCR is shown in Eq. (26) (on top of this page). For SNR, the ratio of RIS to NCR is shown in Eq. (27) (on top of this page). Without loss of generality, we assume that the array elements in RIS and NCR share the same power radiation pattern and gain, i.e., $F_{\mathrm{RIS}}(\theta,\phi)=F_{\mathrm{NCR}}(\theta,\phi)=F(\theta,\phi)$ and $G_{\mathrm{RIS}}=G_{\mathrm{NCR}}=G$. Thus, the received power ratio and SNR ratio of RIS to NCR are as follows:

$$\frac{P_{\mathrm{RIS}}^{\max}}{P_{\mathrm{NCR}}^{\max}}=\underbrace{\frac{B}{M_{\mathrm{NCR}}N_{\mathrm{NCR}}}}_{\text{NCR parameter}}\left(\frac{M_{\mathrm{RIS}}N_{\mathrm{RIS}}}{M_{\mathrm{NCR}}N_{\mathrm{NCR}}}\right)^2\left(\frac{A}{B}\right)^2 \tag{28}$$

and

$$\frac{\gamma_{\mathrm{RIS}}}{\gamma_{\mathrm{NCR}}}=\underbrace{\frac{B}{M_{\mathrm{NCR}}N_{\mathrm{NCR}}}}_{\text{NCR parameter}}\left(\frac{M_{\mathrm{RIS}}N_{\mathrm{RIS}}}{M_{\mathrm{NCR}}N_{\mathrm{NCR}}}\right)^2\left(\frac{A}{B}\right)^2 \cdot\left(1+\underbrace{\frac{G_{\mathrm{R}}\lambda^2}{16\pi^2d_{\mathrm{R}}^2}\frac{\delta^2}{\delta_{\mathrm{R}}^2}}_{\text{system parameter}}\underbrace{GM_{\mathrm{NCR}}N_{\mathrm{NCR}}F(\theta_{\mathrm{R}},\phi_{\mathrm{R}})B}_{\text{NCR parameter}}\right), \tag{29}$$

respectively.

As we can see in Eq. (28), the comparison of received power between RIS and NCR depends on not only the relative array size and magnification but also the parameters of the NCR itself. In a practical scenario, RIS cannot reach the amplification ability of NCR due to its passive reflection characteristics. With the application of MIMO, the NCR parameter $B/(M_{\mathrm{NCR}}N_{\mathrm{NCR}})$ is usually not larger than 1. It is obvious that RIS with a small array size has no advantage over NCR in terms of received power performance. Interestingly, massive array RIS is advantageous for industrial production with quite low energy consumption. On the other hand, NCR with an array as large as the RIS has horrifying energy consumption due to hardware limitations and thus is unsuitable for mass production and application. Therefore, the comparison of the received power between RIS and NCR in a practical parameter setting needs further verification.

For the comparison of SNRs in Eq. (29), the situation is more complicated due to the unclear influence of system parameters. When RIS has better received power performance than NCR, the SNR performance gap can be increased by introducing and magnifying the noise for NCR. When RIS has worse received power performance compared to NCR, it is still possible for RIS to have better SNR performance than NCR in certain conditions. Thus, further verification is still needed for SNR comparison.

3.5 Verification of the theoretical analysis

To further verify the conclusion of theoretical comparison, we simulate the received power and SNR performances for both RIS and NCR.

Considering an NCR of size $K_{\mathrm{NCR}}=8$, the relationship between the NCR amplitude B and the RIS size K_{RIS} according to Eq. (28) is shown in Table 2. Thus, we have Observation 1 (see Section 5) that the received power ratio of RIS to NCR is related to the number of antennas and the amplitude of NCR.

The SNR ratio performance given in Eq. (29) is shown in Fig. 3, where $K_{\mathrm{NCR}}=8$ and $K_{\mathrm{RIS}}=256$. We can see that with the increase of the distance between the repeater and the receiver (d_{R}), the SNR ratio tends to a constant. This indicates that the NCR's amplification of the noise can be ignored when

Table 2 Relationship between NCR amplitude and the RIS size

NCR amplitude (dB)	RIS size	NCR amplitude (dB)	RIS size
0	23	25	403
5	41	30	716
10	72	35	1273
15	128	40	2263
20	227		

RIS: reconfigurable intelligent surface; NCR: network-controlled repeater

the distance between the NCR and the receiver is sufficiently far.

The SNR performances of different repeater-assisted systems are shown in Fig. 4. From Fig. 4a, we can observe that when the NCR is quite near the BS, the SNR has a sudden decrement for downlink transmission. This is because the NCR's relaying power may surpass the maximum transmitting power and thus can relay only the signal at full power. However, RIS does not have this problem. As for the uplink in Fig. 4b, the curves for both RIS and NCR are smooth since the mobile station (MS) often has lower transmitting power.

To summarize the SNR comparison, we have Observation 2 (see Section 5) that the noise introduced and amplified by the NCR can be ignored when the receiver is sufficiently far from the NCR and that the NCR suffers from severe decrease in SNR at downlink when the BS is near due to the constraint of relaying power.

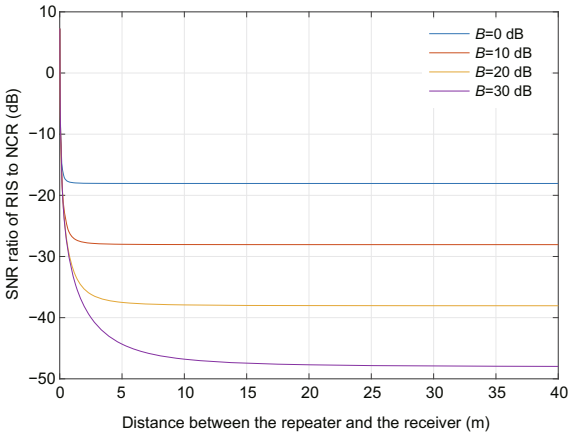

Fig. 3 SNR ratio of RIS to NCR with different NCR amplitudes B (SNR: signal-to-noise ratio; RIS: reconfigurable intelligent surface; NCR: network-controlled repeater). References to color refer to the online version of this figure

4 System-level performance analysis

In this section, we investigate the system-level performance in terms of RSRP and SINR in both the FR1 and FR2 bands.

4.1 Preliminary: parameters and link budget

In this study, we implement a self-developed system-level simulation platform based on C++, which contains more than several hundred classes and tens of thousands of lines of code in total. The system-level simulation platform is developed based on a 5G system simulation that contains the following: (1) network topology; (2) antenna pattern; (3) large-/small-scale channel model; (4) traffic types and service load models; (5) channel measurement and feedback process; (6) resource scheduling (it is assumed that the channels of different users can be irrelevant after a proper resource scheduling scheme we use in system simulation) and uplink power control process; (7) SINR statistic, throughput, delay, spectral efficiency, and other performance indicators.

The simulator can fully support the performance study in 3GPP of various physical layer technologies. The simulation parameters are listed in Table 3.

For system performance metrics, we consider

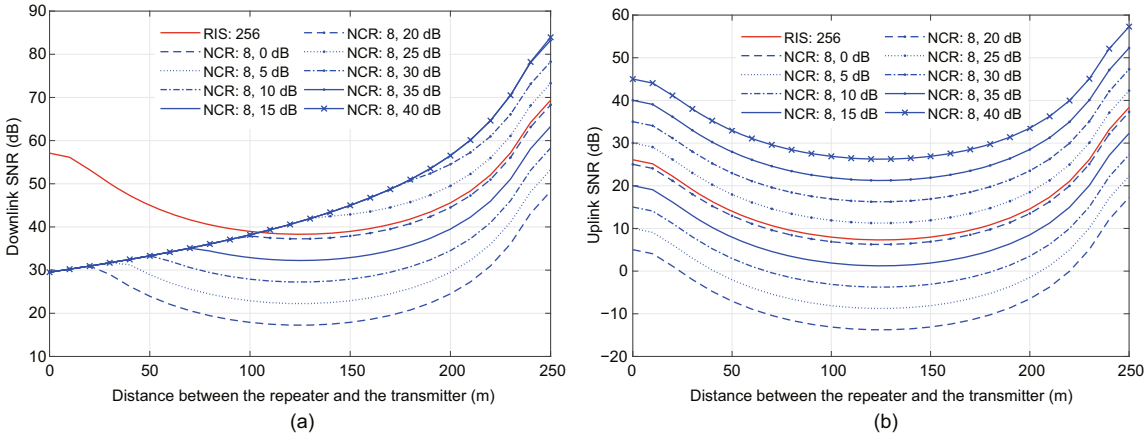

Fig. 4 SNR performance comparison of different repeater-assisted systems: (a) downlink; (b) uplink (SNR: signal-to-noise ratio; RIS: reconfigurable intelligent surface; NCR: network-controlled repeater)

Table 3 Simulation parameters

Parameter	Value
Height of the BS	25 m
Height of the MS	1.5 m
Height of the NCR	5 m
Height of the RIS	15 m
Transmitted power of the BS	43 dBm
Transmitted power of the NCR	30 dBm
Bandwidth	10 MHz
Number of antennas for the BS	8×16
Number of antennas for the MS	1×2
Number of elements per NCR	4×8
Number of elements per RIS	40×40/50×50
Number of NCRs (RISs) per cell	8
Number of MSs per cell	10
Antenna gain of the NCR (RIS)	5 dBi
Position of the NCR	0.95–1.00 cell radius
Position of the RIS	0.95–1.00 cell radius
Position of the MS	0.85–0.90 cell radius

BS: base station; MS: mobile station; RIS: reconfigurable intelligent surface; NCR: network-controlled repeater

RSRP and SINR. To calculate these metrics, two relay modes for NCR are considered, namely, fixed transmission power relay mode and fixed gain relay mode. Under the fixed transmission power relay mode, the NCR gain can be expressed as

$$\begin{aligned} G_{\mathrm{NCR}} =& P_{\mathrm{T,NCR}} - P_{\mathrm{BS-NCR}}^{\mathrm{RSRP}} - N_{\mathrm{BS-NCR}} \\ & - I_{\mathrm{adjBS-NCR}}, \end{aligned} \tag{30}$$

where $P_{\mathrm{T,NCR}}$ is the transmitted power of the NCR, $P_{\mathrm{BS-NCR}}^{\mathrm{RSRP}}$ is the RSRP from the BS to the NCR, $N_{\mathrm{BS-NCR}}$ is the noise from the BS to the NCR, $I_{\mathrm{adjBS-NCR}}$ is the interference from the BS in an adjacent cell to the NCR, and all arguments are in dB. Accordingly, the NCR gain under the fixed gain relay mode satisfies

$$\begin{aligned} G_{\mathrm{NCR}} \leq& P_{\mathrm{T,NCR}} - P_{\mathrm{BS-NCR}}^{\mathrm{RSRP}} - N_{\mathrm{BS-NCR}} \\ & - I_{\mathrm{adjBS-NCR}}. \end{aligned} \tag{31}$$

The total received noise for both RIS- and NCR-assisted systems can be written as

$$N_{\mathrm{MS}} = N_{\mathrm{BS-repeater}} + N_{\mathrm{repeater-MS}}, \tag{32}$$

where the noise from the BS to the repeater and that from the repeater to the MS can be respectively written as

$$\begin{cases} N_{\mathrm{BS-repeater}} = -174\ \mathrm{dBm/Hz} + F_{\mathrm{repeater}} + B, \\ N_{\mathrm{repeater-MS}} = N_{\mathrm{BS-repeater}} + F_{\mathrm{repeater}} + F_{\mathrm{MS}} \\ \qquad\qquad -174\ \mathrm{dBm/Hz} + B, \end{cases} \tag{33}$$

where F_{repeater} and F_{MS} are noise figures, and B is the bandwidth in dB. Then, the RSRP from the BS to the repeater is

$$P_{\mathrm{BS-repeater}}^{\mathrm{RSRP}} = P_{\mathrm{T,BS}} + L_{\mathrm{BS-repeater}}, \tag{34}$$

where $P_{\mathrm{T,BS}}$ is the transmitted power of the BS in dB and $L_{\mathrm{BS-repeater}}$ is the BS–repeater coupling loss in dB. The RSRP from the repeater to the MS is

$$P_{\mathrm{repeater-MS}}^{\mathrm{RSRP}} = G_{\mathrm{repeater}} + P_{\mathrm{BS-repeater}}^{\mathrm{RSRP}} + L_{\mathrm{MS-repeater}}, \tag{35}$$

where G_{repeater} is the repeater gain. The RSRP from the BS to the MS is

$$P_{\mathrm{BS-MS}}^{\mathrm{RSRP}} = P_{\mathrm{T,BS}} + L_{\mathrm{MS-repeater}}. \tag{36}$$

The total RSRP is

$$P_{\mathrm{total}}^{\mathrm{RSRP}} = P_{\mathrm{BS-MS}}^{\mathrm{RSRP}} + P_{\mathrm{repeater-MS}}^{\mathrm{RSRP}}. \tag{37}$$

Thus, the SINR can be written as

$$\begin{aligned} \mathrm{SINR} =& P_{\mathrm{total}}^{\mathrm{RSRP}} / (N_{\mathrm{MS}} + I_{\mathrm{BS-MS}} + I_{\mathrm{adjBS-adjrepeater-MS}} \\ & + I_{\mathrm{adjBS-repeater-MS}}), \end{aligned} \tag{38}$$

where $I_{\mathrm{BS-MS}}$ is the direct link interference, $I_{\mathrm{adjBS-adjrepeater-MS}}$ is the interference from the BS–repeater link in an adjacent cell, $I_{\mathrm{adjBS-repeater-MS}}$ is the interference from an adjacent BS to the local repeater, and all arguments are linear.

4.2 Performance in the FR1 band

In this subsection, we present the RSRP and SINR simulation results from the comparison between RIS and NCR under the FR1 band. Specifically, we consider a typical 2.6-GHz carrier in the FR1 band. In a low-frequency band such as FR1, NCR amplifies only the signal without beamforming. However for RIS, the reflecting characteristics naturally transmit the signal to a specific direction. The total performance comparison can be seen in Table 4.

The cumulative distribution functions (CDFs) of the RSRPs of different repeater-assisted systems in the FR1 band are shown in Fig. 5. We can observe that NCR surpasses RIS in RSRP performance for both full-power and fixed 40-dB gain relay modes. As summarized in Table 4, the relaying power exceeds the maximum power by 45% and 9% for fixed 40 dB and 30 dB, respectively. Thus, we have Observation 3 (see Section 5) that the RSRP of NCR

can surpass that of RIS in certain system parameter settings and that the relative gain can be improved for RIS when the number of array elements increases.

The SINR performances of different repeater-assisted systems in the FR1 band are shown in Fig. 6. We can observe from Fig. 6a that the SINR performance of RIS always surpasses that of NCR under the parameter settings in Table 3. This is because NCR amplifies not only the signal power but also noise and interference, as shown in Fig. 6b. Thus, we have Observation 4 (see Section 5) that the SINR performance of RIS always surpasses that of NCR because NCR amplifies noise and interference simultaneously.

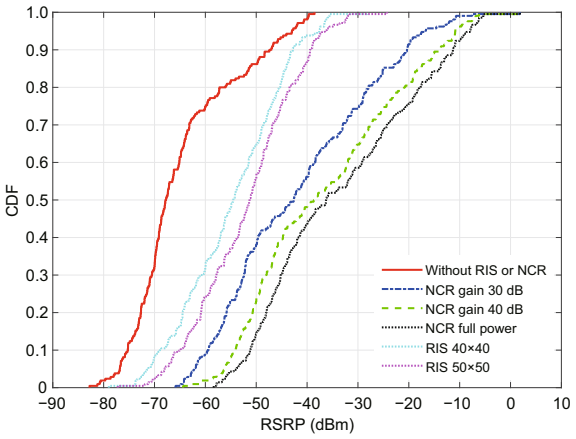

Fig. 5 CDFs of the RSRP at 2.6 GHz (CDF: cumulative distribution function; RSRP: reference signal received power; RIS: reconfigurable intelligent surface; NCR: network-controlled repeater)

4.3 Performance in the FR2 band

In this subsection, we present the RSRP and SINR simulation results from the comparison between RIS and NCR under the FR2 band. Specifically, we consider a typical 26-GHz carrier in the FR2 band. In the simulation, RIS considers user-specific beamforming, while NCR implements beam sweeping.

The RSRP CDFs of different repeater-assisted systems in the FR2 band are shown in Fig. 7. We can observe that NCR suffers from RSRP performance

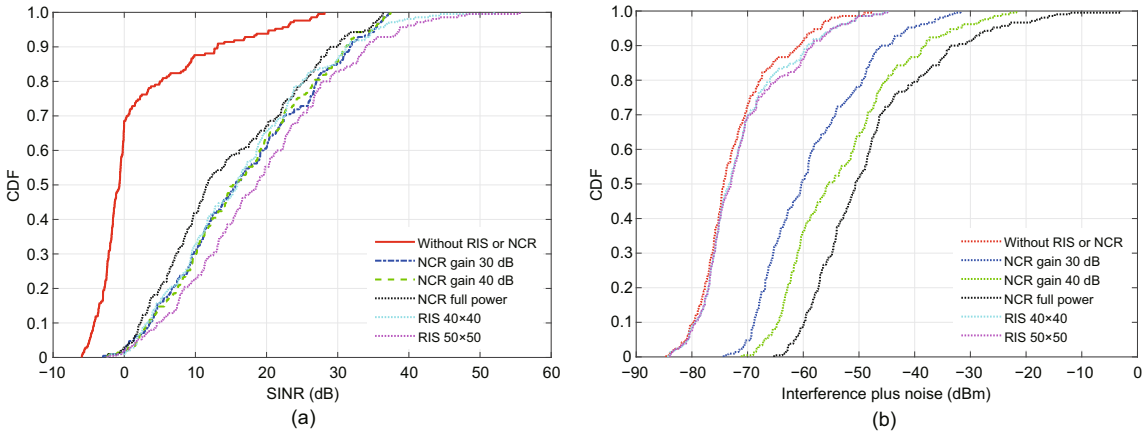

Fig. 6 SINR performance comparison of different repeater-assisted systems, where the carrier frequency is 2.6 GHz: (a) CDFs of the SINR; (b) CDFs of the noise and interference (SINR: signal-to-interference-and-noise ratio; CDF: cumulative distribution function; RIS: reconfigurable intelligent surface; NCR: network-controlled repeater)

Table 4 Performance comparison between RIS and NCR in the FR1 band

Repeater	Average gain in RSRP (dB)	Average gain in SINR (dB)	Repeater relaying power exceeding the maximum power	Noise and interference amplification (dB)
NCR full power	24.63	3.86		20.57
NCR gain 40 dB	21.37	4.44	≈ 45%	17.14
NCR gain 30 dB	15.13	4.23	≈ 9%	11.43
RIS 40 × 40	14.63	13.78		
RIS 50 × 50	17.70	16.93		

RSRP: reference signal received power; SINR: signal-to-interference-and-noise ratio; RIS: reconfigurable intelligent surface; NCR: network-controlled repeater

degradation in the FR2 band compared to that in the FR1 band. This is because in applications, NCR implements beam sweeping and thus is not able to achieve fine alignment. On the other hand, RIS implements a preset user-specific reflection codebook. Thus, we have Observation 5 (see Section 5) that RIS can be more accurate in terms of beam alignment compared to NCR.

The SINR performances of different repeater-assisted systems in the FR2 band are shown in Fig. 8. We can observe from Fig. 8a that the SINR of NCR surpasses that of RIS. The gap between RIS and NCR in terms of interference plus noise narrows in the FR2 band when comparing Fig. 8b with Fig. 6b. The main difference between FR1 and FR2 is that beamforming is considered in FR2. Therefore, the increased SINR performance of NCR in FR2 is because of the beam sweeping for NCR, which can efficiently decrease the interference.

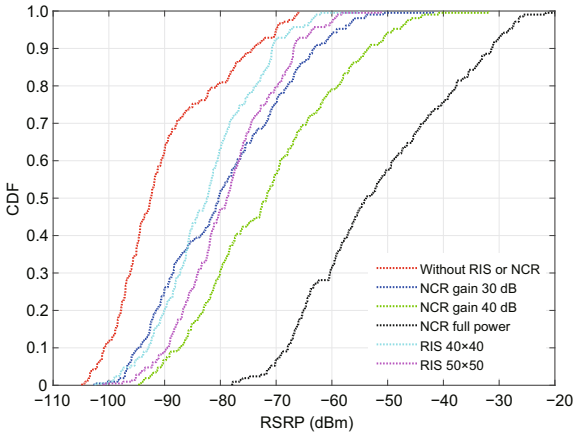

Fig. 7 CDFs of the RSRP at 26 GHz (CDF: cumulative distribution function; RSRP: reference signal received power; RIS: reconfigurable intelligent surface; NCR: network-controlled repeater)

5 Observations on the performance comparison between RIS and NCR

According to the above analysis and simulation results, the observations of the performance comparison between RIS and NCR can be summarized as follows:

Observation 1 The received power ratio of RIS to NCR is related to the number of antennas and the amplitude of NCR.

Observation 2 The noise introduced and amplified by the NCR can be ignored when the receiver is sufficiently far from the NCR, and the NCR suffers from severe decrease in SNR at downlink when the BS is near due to the constraint of relaying power.

Observation 3 In the FR1 band, NCR amplifies only the signal without beamforming. The RSRP of the NCR can surpass that of RIS in certain system parameter settings and the relative gain can be improved for the RIS when the number of array elements increases.

Observation 4 In the FR1 band, NCR amplifies only the signal without beamforming. The SINR performance of RIS always surpasses that of NCR because NCR amplifies noise and interference simultaneously.

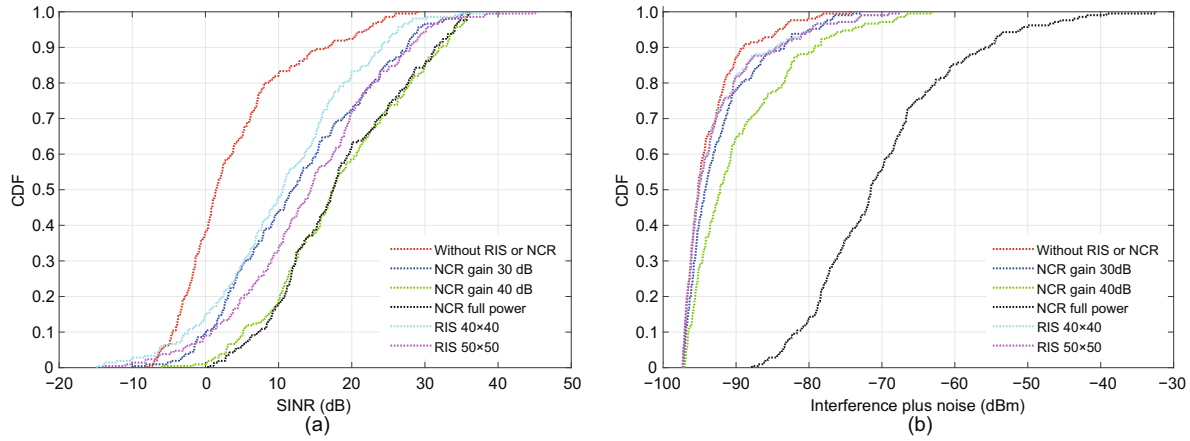

Fig. 8 SINR performance comparison of different repeater-assisted systems, where the carrier frequency is 26 GHz: (a) CDFs of the SINR; (b) CDFs of the noise and interference (SINR: signal-to-interference-and-noise ratio; CDF: cumulative distribution function; RIS: reconfigurable intelligent surface; NCR: network-controlled repeater)

Observation 5 In the FR2 band, RIS can be more accurate in terms of beam alignment compared to NCR.

Considering engineering applications, there are more observations when comparing RIS with NCR.

Observation 6 In terms of deployment and application scenarios, RIS can be more flexible than NCR because of the energy-saving characteristic. Because of the passive reflection, it is possible for RIS to be deployed with portable power sources. On the other hand, NCR consists of massive amplifiers and thus highly relies on sufficient power supply. Therefore, the deployment and application of NCR can have more constraints compared to the case of RIS.

Observation 7 In terms of protocol architecture and control methods, RIS needs more attention in terms of the design of low power consumption and low complexity in contrast with the NCR. This is also because of the passive reflection of RIS. A typical application is the semi-passive RIS, which plugs into the powerlines for beam training while needing little power supply when operating as a relay.

6 Conclusions

In this paper, we compared the performances of RIS and NCR. We first analyzed the theoretical received power and SNR performances for both RIS and NCR and validated the performances in link-level simulation. Then, we simulated the RSRP and SINR performances at the system level for both RIS and NCR in the FR1 and FR2 bands. The simulation results gave several insights into engineering applications:

1. In FR1, RIS can surpass NCR in terms of RSRP in certain system parameter settings. The SINR performance for RIS can be better than that of NCR.

2. In FR2, NCR can surpass RIS in terms of both RSRP and SINR in certain system parameter settings.

3. RIS is more flexible than NCR in context of deployment and applications. However, RIS needs more attention in the designing of the protocol architecture and the control methods.

Our future work includes the influence of channel estimation error on RIS and NCR, and the protocol architecture and control methods of RIS.

Contributors

Yiwei SUN and Xin SU designed the research. Boyang DUAN and Hanning WANG processed the data. Yiwei SUN drafted the paper. Xin SU and Qi GU helped organize the paper. Jing JIN and Yifei YUAN revised and finalized the paper.

Compliance with ethics guidelines

Yiwei SUN, Boyang DUAN, Xin SU, Hanning WANG, Qi GU, Jing JIN, and Yifei YUAN declare that they have no conflict of interest.

Data availability

The data that support the findings of this study are available from the corresponding author upon reasonable request.

References

3GPP, 2021. SI: Study on NR Network-Controlled Repeaters. Technical Report No. RP-213700, 3GPP, Geneva. Available from https://www.3gpp.org/ftp/tsg_ran/TSG_RAN/TSGR_94e/Docs [Accessed on Aug. 20, 2023].

3GPP, 2022a. On the Side Control Information and Performance Evaluation for NCR. Technical Report No. R1-2105875, 3GPP, Geneva. Available from https://www.3gpp.org/ftp/tsg_ran/WG1_RL1/TSGR1_110/Docs [Accessed on Aug. 20, 2023].

3GPP, 2022b. Study on Channel Model for Frequencies from 0.5 to 100 GHz. Technical Report No. 38.901, 3GPP, Geneva. Available from ftp://www.3gpp.org/Specs/archive/38_series/38.901/ [Accessed on Aug. 20, 2023].

Askar R, Chung J, Guo ZH, et al., 2021. Interference handling challenges toward full duplex evolution in 5G and beyond cellular networks. *IEEE Wirel Commun*, 28(1):51-59. https://doi.org/10.1109/MWC.001.2000228

Ayoubi RA, Mizmizi M, Tagliaferri D, et al., 2023. Network-controlled repeaters vs. reconfigurable intelligent surfaces for 6G mmW coverage extension. https://doi.org/10.48550/arXiv.2211.08033

Basar E, 2020. Reconfigurable intelligent surface-based index modulation: a new beyond MIMO paradigm for 6G. *IEEE Trans Commun*, 68(5):3187-3196. https://doi.org/10.1109/TCOMM.2020.2971486

Basar E, Di Renzo M, De Rosny J, et al., 2019. Wireless communications through reconfigurable intelligent surfaces. *IEEE Access*, 7:116753-116773. https://doi.org/10.1109/ACCESS.2019.2935192

Basar E, Yildirim I, Kilinc F, 2021. Indoor and outdoor physical channel modeling and efficient positioning for reconfigurable intelligent surfaces in mmWave bands. *IEEE Trans Commun*, 69(12):8600-8611. https://doi.org/10.1109/TCOMM.2021.3113954

Björnson E, Özdogan Ö, Larsson EG, 2020a. Intelligent reflecting surface versus decode-and-forward: how large surfaces are needed to beat relaying? *IEEE Wirel*

Commun Lett, 9(2):244-248. https://doi.org/10.1109/LWC.2019.2950624

Björnson E, Özdogan Ö, Larsson EG, 2020b. Reconfigurable intelligent surfaces: three myths and two critical questions. *IEEE Commun Mag*, 58(12):90-96. https://doi.org/10.1109/MCOM.001.2000407

Cui TJ, Qi MQ, Wan X, et al., 2014. Coding metamaterials, digital metamaterials and programmable metamaterials. *Light Sci Appl*, 3(10):e218. https://doi.org/10.1038/lsa.2014.99

Gu Q, Wu D, Su X, et al., 2021. Performance comparisons between reconfigurable intelligent surface and full/half-duplex relays. Proc IEEE 94th Vehicular Technology Conf, p.1-6. https://doi.org/10.1109/VTC2021-FALL52928.2021.9625201

Gui G, Liu M, Tang FX, et al., 2020. 6G: opening new horizons for integration of comfort, security, and intelligence. *IEEE Wirel Commun*, 27(5):126-132. https://doi.org/10.1109/MWC.001.1900516

Guo H, Madapatha C, Makki B, et al., 2023. A comparison between network-controlled repeaters and reconfigurable intelligent surfaces. https://doi.org/10.48550/arXiv.2211.06974

Han Y, Tang WK, Jin S, et al., 2019. Large intelligent surface-assisted wireless communication exploiting statistical CSI. *IEEE Trans Veh Technol*, 68(8):8238-8242. https://doi.org/10.1109/TVT.2019.2923997

Huang CW, Zappone A, Alexandropoulos GC, et al., 2019. Reconfigurable intelligent surfaces for energy efficiency in wireless communication. *IEEE Trans Wirel Commun*, 18(8):4157-4170. https://doi.org/10.1109/TWC.2019.2922609

Hum SV, Perruisseau-Carrier J, 2014. Reconfigurable reflectarrays and array lenses for dynamic antenna beam control: a review. *IEEE Trans Antenn Propag*, 62(1):183-198. https://doi.org/10.1109/TAP.2013.2287296

Jian MN, Alexandropoulos GC, Basar E, et al., 2022. Reconfigurable intelligent surfaces for wireless communications: overview of hardware designs, channel models, and estimation techniques. *Intell Conv Netw*, 3(1):1-32. https://doi.org/10.23919/ICN.2022.0005

Khaleel A, Basar E, 2021. Reconfigurable intelligent surface-empowered MIMO systems. *IEEE Syst J*, 15(3):4358-4366. https://doi.org/10.1109/JSYST.2020.3011987

Leone G, Moro E, Filippini I, et al., 2022. Towards reliable mmWave 6G RAN: reconfigurable surfaces, smart repeaters, or both? Proc 20th Int Symp on Modeling and Optimization in Mobile, Ad Hoc, and Wireless Networks, p.81-88. https://doi.org/10.23919/WiOpt56218.2022.9930587

Li QC, El-Hajjar M, Hemadeh I, et al., 2023a. Reconfigurable intelligent surface aided amplitude- and phase-modulated downlink transmission. *IEEE Trans Veh Technol*, 72(6):8146-8151. https://doi.org/10.1109/TVT.2023.3239545

Li QC, El-Hajjar M, Hemadeh I, et al., 2023b. The reconfigurable intelligent surface-aided multi-node IoT downlink: beamforming design and performance analysis. *IEEE Int Things J*, 10(7):6400-6414. https://doi.org/10.1109/JIOT.2022.3225127

Liu RQ, Wu QQ, Di Renzo M, et al., 2022. A path to smart radio environments: an industrial viewpoint on reconfigurable intelligent surfaces. *IEEE Wirel Commun*, 29(1):202-208. https://doi.org/10.1109/MWC.111.2100258

Ntontin K, Di Renzo M, Lazarakis F, 2020. On the rate and energy efficiency comparison of reconfigurable intelligent surfaces with relays. Proc IEEE 21st Int Workshop on Signal Processing Advances in Wireless Communications, p.1-5. https://doi.org/10.1109/SPAWC48557.2020.9154308

Pan CH, Ren H, Wang KZ, et al., 2021. Reconfigurable intelligent surfaces for 6G systems: principles, applications, and research directions. *IEEE Commun Mag*, 59(6):14-20. https://doi.org/10.1109/MCOM.001.2001076

Qualcomm, 2021. NR Smart Repeaters. Technical Report No. RWS-210019. Available from https://www.3gpp.org/ftp/tsg_ran/TSG_RAN/TSGR_AHs/2021_06_RAN_Rel18_WS/Docs [Accessed on Aug. 20, 2023].

RISTA, 2023. Reconfigurable intelligent surface technology white paper. RIS TECH Alliance. https://doi.org/10.12142/RISTA.202302002

Tang WK, Dai JY, Chen MZ, et al., 2020. MIMO transmission through reconfigurable intelligent surface: system design, analysis, and implementation. *IEEE J Sel Areas Commun*, 38(11):2683-2699. https://doi.org/10.1109/JSAC.2020.3007055

Tang WK, Chen MZ, Chen XY, et al., 2021. Wireless communications with reconfigurable intelligent surface: path loss modeling and experimental measurement. *IEEE Trans Wirel Commun*, 20(1):421-439. https://doi.org/10.1109/TWC.2020.3024887

Wu QQ, Zhang R, 2019. Intelligent reflecting surface enhanced wireless network via joint active and passive beamforming. *IEEE Trans Wirel Commun*, 18(11):5394-5409. https://doi.org/10.1109/TWC.2019.2936025

Wu QQ, Zhang R, 2020. Towards smart and reconfigurable environment: intelligent reflecting surface aided wireless network. *IEEE Commun Mag*, 58(1):106-112. https://doi.org/10.1109/MCOM.001.1900107

Yildirim I, Uyrus A, Basar E, 2021. Modeling and analysis of reconfigurable intelligent surfaces for indoor and outdoor applications in future wireless networks. *IEEE Trans Commun*, 69(2):1290-1301. https://doi.org/10.1109/TCOMM.2020.3035391

Yuan J, Wen MW, Li Q, et al., 2021. Receive quadrature reflecting modulation for RIS-empowered wireless communications. *IEEE Trans Veh Technol*, 70(5):5121-5125. https://doi.org/10.1109/TVT.2021.3073161

Yuan YF, Wu D, Huang YH, et al., 2022. Reconfigurable intelligent surface relay: lessons of the past and strategies for its success. *IEEE Commun Mag*, 60(12):117-123. https://doi.org/10.1109/MCOM.003.2200193

Zhang SW, Zhang R, 2020. Capacity characterization for intelligent reflecting surface aided MIMO communication. *IEEE J Sel Areas Commun*, 38(8):1823-1838. https://doi.org/10.1109/JSAC.2020.3000814

List of supplementary materials

1 Proof of Proposition 1

2 Proof of Proposition 2